CORRUGATED STRUCTURE INSERTION TO EXTEND SASE BANDWIDTH UP TO 3% AT THE EUROPEAN XFEL

I. Zagorodnov*, G. Feng, T. Limberg, Deutsches Elektronen-Synchrotron, Hamburg, Germany

Abstract

The usage of x-ray free electron laser (XFEL) in femtosecond nanocrystallography involves sequential illumination of many small crystals of arbitrary orientation. Hence a wide radiation bandwidth could be useful in order to obtain and to index a larger number of Bragg peaks used for determination of crystal orientation.

Considering the baseline configuration of the European XFEL in Hamburg, and based on beam dynamics simulations, we demonstrate here that usage of corrugated structures allows for a considerable increase in radiation bandwidth. It allows for data collection with a 3% bandwidth, a few micrjoule radiation pulse energy, a few fs pulse duration, and a photon energy 5.4 keV.

INTRODUCTION

The usage of x-ray free electron laser (XFEL) in femtosecond nanocrystallography involves sequential illumination of many small crystals of arbitrary orientation and a wide radiation bandwidth could be useful for determination of crystal orientation. With nominal scenario for beam compression and transport at the European XFEL [1] the radiation bandwidth is quite narrow, on the level of several permilles.

It was shown in [2] that a strong beam compression could be used to increase the correlated energy spread of the electron beam and as consequence to increase the radiation bandwidth up to 2 % at photon energy 6 keV. In this paper we study another possibility: we use over-compression of the electron beam at the last chicane and insert corrugated structures before the undulator section to generate strong wakefields [3].

Based on beam dynamics simulations, we demonstrate here that the usage of corrugated structures allows for a tenfold increase in radiation bandwidth.

BEAM DYNAMICS IN LINAC

Figure 1: Layout of the European XFEL.

The European XFEL is under construction now in Hamburg. It contains several photon lines to produce extremely short and bright light pulses with wave length down to 0.04

---

* Igor.Zagorodnov@desy.de

nm. The layout of the accelerator (with the undulator line SASE1) is shown in Fig. 1. Beam dynamics in the accelerator with nominal set of parameters is described in [4].

In this paper we consider a special scenario with over-compression of the electron bunch in the last bunch compressor (BC2 in Fig. 1). The over-compression allows to obtain a bunch with lower particle energy at the tail. This energy difference will be enhanced later on by strong wake fields of the corrugated structures.

The setup of simulations can be found in [5]. For the numerical modeling of the linac we have used two codes: code ASTRA [6] for straight sections and code CSRtrack [7] for curved parts of the beam trajectory. Code ASTRA allows to take into account three dimensional space-charge fields, but it neglects the radiation. Code CSRtrack is used to model coherent synchrotron radiation in the dispersion sections. In order to include the effect of the vacuum chamber we have applied the concept of wake fields. The wake functions for a point charge at different linac components are obtained with the code ECHO [8]. The impact of wake fields has been modeled through discrete kicks at several positions along the linac.
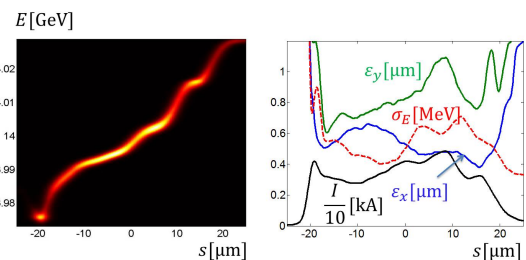
Figure 2: Beam after collimator.

The longitudinal phase space and the slice parameters of the beam after collimator section are shown in Fig. 2. The tail has an energy drop of about 55 MeV.

It is well known, that the spectrum bandwidth of self-amplified spontaneous emission (SASE) radiation is approximately equal to the doubled energy bandwidth in the electron beam. For the final beam energy of 14 GeV the relative energy bandwidth in the electron beam is about 0.4% and we can hope to have the SASE radiation bandwidth of 0.8%. In order to increase the bandwidth up to several percents we will use a chain of corrugated structures. In our studies the corrugate structure has the parameters suggested at SLAC.
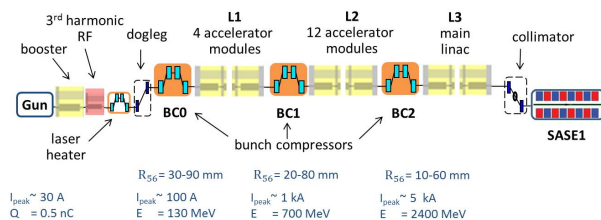
WAKE IN CORRUGATED STRUCTURE

The geometry of the corrugated structure is shown in Fig. 3. Here $p = h = 2t = 0.5$mm, plate halfwidth $w = 6$mm

(in x-direction), halfaperture $a = 0.7$mm, structure length $L = 2$m.

In this paper we use a *modal* expression derived in [5]. The main difference between the previous model [9] and the present one is that the former was for a structure composed of two parallel, corrugated plates, where the impedance is continuous; the present model is for the same structure but with perfectly conducting side walls, so that the impedance is given by an infinite sum of modes.
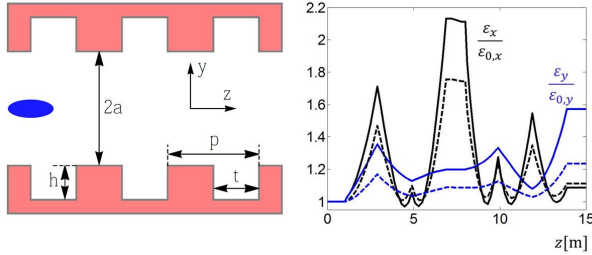
Figure 3: Corrugated structure (left) and emittance growth (right).

The longitudinal wake function for arbitrary offsets of the source and the witness particles can be written as

$$w_z = \frac{1}{w} \sum_{m=1}^{\infty} w_z(k_{x,m}) \sin(k_{x,m} x_0) \sin(k_{x,m} x), \quad (1)$$

$$w_z(k_x) = w_z^{cc}(k_x, s) \cosh(k_x y_0) \cosh(k_x y) + \\ + w_z^{ss}(k_x, s) \sinh(k_x y_0) \sinh(k_x y),$$

$$w_z^{cc}(k_x, s) = \frac{Z_0 c X}{a \sinh(2X)} e^{-\frac{X}{\tanh(X)} \sqrt{\frac{s}{4s_0}}},$$

$$w_z^{ss}(k_x, s) = \frac{Z_0 c X}{a \sinh(2X)} e^{-\frac{X}{\coth(X)} \sqrt{\frac{s}{4s_0}}}, \quad (2)$$

$$k_{x,m} = \frac{\pi}{2w} m, \qquad X = a k_x,$$

where x_0, y_0, x, y are transverse coordinates of the source and the witness particles, $s = z_0 - z$ is the distance in the longitudinal coordinate between the particles. To define the parameter s_0 we have done sets of simulations and found $s_0 = 0.12$mm. We note that the same value for s_0 can be found from the simple equation $s_0 = 0.41 a^{1.8} t^{1.6} p^{-2.4}$, obtained earlier in [10] for the chain of pillboxes.

The high frequency limit of the impedance was considered in [11]. At this limit the both modal coefficients reduce to the same expression

$$w_z^{cc}(k_x, s) = w_z^{ss}(k_x, s) = \frac{Z_0 c X}{a \sinh(2X)}. \quad (3)$$

In order to confirm the accuracy of the introduced wake function, we have done in code ECHO the direct calculation of the wake potential for a "pencil" bunch with the same longitudinal current profile as obtained from "start-to-end" (S2E) simulations. The results of this calculation are shown in Fig. 4. Here we plot the results for Eq. (2) (red curve) and compare with Eq. (3) (blue curve) and with the direct numerical solution (black curve).
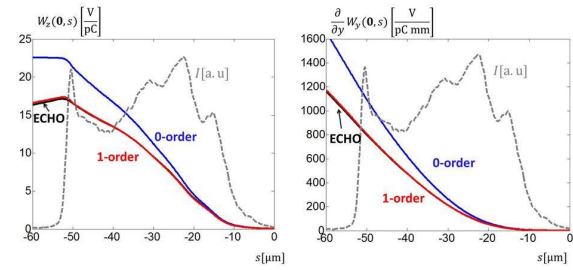
Figure 4: The longitudinal and the transverse quadrupole wake potentials on the axis.

BEAM DYNAMICS IN INSERTION

In this section we present results of particle tracking through the setup shown in Fig. 5. The setup consists of 6 corrugated structures with one quadrupole in the middle. To compensate the defocussing effect of the "quadrupole" component of the wake, shown in Fig. 4, the neighbor corrugated structure modules are rotated by 90 degree.
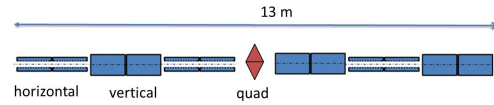
Figure 5: Layout of the corrugated structure insertion.

In order to model the beam dynamics in the presence of the wakefields we have used the open source code OCELOT [12]. We have developed and tested the wake field module. The implementation follows the approach described in [13, 14].

For testing of the numerical implementation we have compared the results from code OCELOT with the analytical estimations presented in [11]. The parameters used in these equations can be found in [5]. In this example we apply only one kick in OCELOT without particle tracking. As we see from Table 1 the numerical and the analytical results for "zeroth"-order approximation agree. But they overestimate considerably the real wake field effects. The wake described accurately with "first"-order approximation is given in the last column of Table 1. The energy loss in tail introduced by one module is only 35 MeV. Hence in order to introduce 1.5% of additional energy loss at 14 GeV we need at least 6 modules.

Table 1: Numerical Results vs. Analytical Estimations [11]

Parameter name	from [11]	"0th"	"1st"
Emitt. growth	1.484	1.479	1.29
Energy spread (tail), keV	80.2	81.0	56
Energy loss (tail), MeV	45.3	45.0	35

In the following we additionally consider the "ideal" beam with a rectangular longitudinal profile, without energy chirp and with constant slice parameters listed in [5].

The tracking is done through the setup of Fig. 5. In Fig. 3 we show the projected emittance growth along the insertion.

Table 2: Impact of the Insertion on the Beam Parameters

Parameter name	"ideal"	"s2e"
Init./final x-emittance, μm	0.64/0.70	0.72/0.77
Init./final y-emittance, μm	1.09/1.33	1.18/1.82
Init./final tail loss, MeV	0/212	55/255

About 60% of growth in the vertical emittance can be seen. This increase in the projected emittance cannot be corrected and it will result in the slice mismatch along the beam at the undulator. Impossibility to match all slices along the beam will reduce the SASE radiarion power. There is almost no change in the electron beam slice parameters. The final increase of slice energy spread at the bunch tail is negligible. The changes in the main parameters of the beam after the insertion are summarized in Table 2.

BROADBAND SASE RADIATION

In this section we consider the properties of SASE radiation in the undulator lines SASE1/SASE2. The parameters of the undulators are listed in [15]. With the nominal scenario of the bunch compression and the transport the electron bunch with charge 0.5 nC and energy 14 GeV will have only about several MeV of energy spread and will produce the SASE radiation with "full-width-half-maximum" (FWHM) bandwidth 0.2% at photon energy of 4.96 keV. With the scenario described in this paper the energy difference between the tail and the head is increased to 255 MeV.

In our FEL simulations we use code ALICE [16]. The undulator wavelength is 40 mm, the averaged undulator parameter is 2.76, the radiation wavelength is 0.23 nm, the averaged β-function is 16 m.
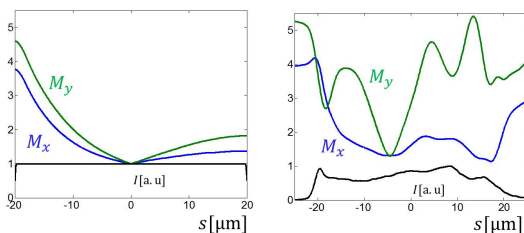
Figure 6: The mismatch parameters of the "ideal"(left) and the "s2e" (right) bunches at the undulator entrance.
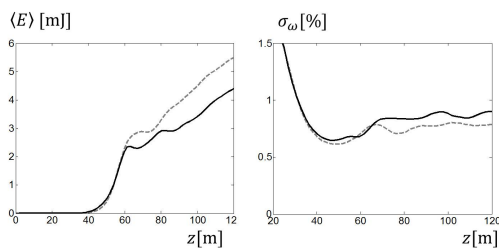
Figure 7: The radiation energy (left) and the RMS bandwidth (right): solid line -"s2e" beam, dashed line -"ideal" beam.
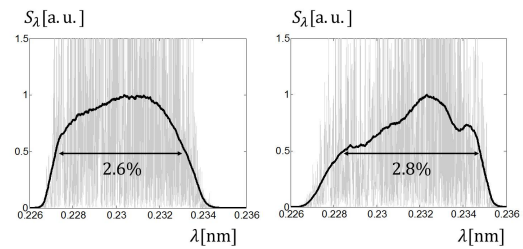
Figure 8: The radiation spectrum at z=115 m for "ideal" (left) and "s2e"(right) beams.

In Fig. 6 we show the beta mismatch parameters [17] along the beam matched to the undulator entrance.The beam from the "s2e" simulations has a larger mismatch at the head and at the tail. The case shown in Fig. 6 is obtained when we reduce the mismatch parameters along the whole bunch.

The active length of the undulator is 175 meters. With the electron beams considered the SASE saturation is reached at the position $z = 60$ m. In the left plot in Fig. 7 we show the averaged energy in the photon pulse along the undulator line. The radiation pulse energy at the saturation is about 3 mJ. We do not use any undulator tapering and do not take into account the undulator wake fields in this study. The tapering could increase the radiation power yet by order of magnitude but the radiation bandwidth can be reduced because of it.

The RMS radiation bandwidth along the undulator section is shown in the right plot in Fig. 7. It reaches 0.9% at position $z = 120$ m. The radiation spectrum has not Gaussian shape. In Fig. 8 we show the spectrum at position $z = 115$ m. The FWHM radiation bandwidth reaches here 2.8% for the electron beam from "start-to-end" simulations. The solid lines present the spectrum averaged over many shots. The oscillating gray lines show an one shot spectrum.

REFERENCES

[1] M. Altarelli *et al.* (Eds), Report No. DESY 2006-097, 2006.

[2] S. Serkez *et al.*, Report No. DESY 13-109, Hamburg, 2013.

[3] K. Bane and G. Stupakov, *Nucl. Inst. Meth.* A **690** 106, 2012.

[4] G. Feng *et al.*, TESLA-FEL 2013-04, Hamburg, 2013.

[5] I. Zagorodnov *et al.*, *NIM* A **837** 69, 2016.

[6] K. Floettmann, *ASTRA. User's Manual*, Hamburg, 2014.

[7] M. Dohlus and T. Limberg, *CSRtrack, User's Manual*, 2012.

[8] I. Zagorodnov and T. Weiland, *PR STAB* **8** 042001, 2005.

[9] K. Bane *et al.*, SLAC-PUB-16497, DESY 16-056, 2016.

[10] K.L.F. Bane *et al.*, Report No. SLAC-PUB-7862, 1998.

[11] K. Bane and G. Stupakov, *NIM* A **820** 156, 2016.

[12] I. Agapov *et al.*, *NIM* A, **768**, 2014.

[13] O. Zagorodnova *et al.*, in *Proc. PAC'09*, Vancouver, Canada.

[14] M. Dohlus *et al.*, Report No. DESY 12-012, 2012.

[15] J. Pflueger, talk at XFEL Meeting 13.04.2016.

[16] I. Zagorodnov, in *Proc. ICAP'11*, Rostock, Germany, p. 81.

[17] M. Sands, Report No. SLAC-AR-85 April, 1991.